

Article

# Robust Sliding Mode Control of a Unipolar Power Inverter

Muhammad Awais <sup>1</sup>, Abdul Rehman Yasin <sup>1,\*</sup>, Mudassar Riaz <sup>1</sup>, Bilal Saqib <sup>1</sup>, Saba Zia <sup>1</sup> and Amina Yasin <sup>2</sup>

<sup>1</sup> Department of Electrical Engineering, The University of Lahore, Lahore 54000, Pakistan; ramay2929@gmail.com (M.A.); mudassarriaz041@gmail.com (M.R.); bilalsaqib@gmail.com (B.S.); saba.zia@gmail.com (S.Z.)

<sup>2</sup> Department of Basic Sciences, Preparatory Year Deanship, King Faisal University, Al Hofuf 31982, Saudi Arabia; amnagyasini@gmail.com

\* Correspondence: metary@gmail.com; Tel.: +92-321-4511396

**Abstract:** The key issue in the practical implementation of the sliding mode (SM) control-based power inverter is the variable switching frequency. This variable switching frequency not only induces electromagnetic interference (EMI) noise, but also reduces the efficiency of the inverter, as the size of the inductor and capacitor does not alter in tandem with this variable frequency. In this context, fixed switching frequency-based SM control techniques are proposed; however, some of them are too complex, while others compromise the inherent properties of SM control. In this research, a fixed frequency SM controller is proposed, which is based on the novel low-pass filter extraction of the discontinuous control signal. This allows the technique to be implemented with fewer hardware components, thus reducing the complications of implementation, while maintaining the robustness and parametric invariance of SM control. A simulation-based comparison with an existing pulse width modulated (PWM) SM controller is presented as the benchmark. In comparison with the sigmoid function SM controller, an improvement of 50% in the settling time along with zero steady-state errors and a further 37% and 42% improvement in the undershoot and overshoot, respectively, is reported in the simulation. A hardware setup is established to validate the proposed technique, which substantiates the simulation results and its disturbance rejection properties.

**Keywords:** fixed frequency sliding mode control; unipolar single phase inverter; pulse width modulation (PWM); filter extracted equivalent control (FEEC)



**Citation:** Awais, M.; Yasin, A.R.; Riaz, M.; Saqib, B.; Zia, S.; Yasin, A. Robust Sliding Mode Control of a Unipolar Power Inverter. *Energies* **2021**, *14*, 5405. <https://doi.org/10.3390/en14175405>

Academic Editors: Ramkrishan Maheshwari and Ahmed Abu-Siada

Received: 22 June 2021

Accepted: 24 August 2021

Published: 31 August 2021

**Publisher's Note:** MDPI stays neutral with regard to jurisdictional claims in published maps and institutional affiliations.



**Copyright:** © 2021 by the authors. Licensee MDPI, Basel, Switzerland. This article is an open access article distributed under the terms and conditions of the Creative Commons Attribution (CC BY) license (<https://creativecommons.org/licenses/by/4.0/>).

## 1. Introduction

Over the past decade, energy requirements have increased exponentially, and the increased use of conventional energy sources has had a detrimental effect on the environment. This has shifted the research focus toward renewable energy resources. Since solar energy is most abundant in nature, among other renewable energy resources, photovoltaic generation systems have emerged. Single-phase pulse width modulation (PWM)-based unipolar inverters are an integral component for the realization of such systems. However, the non-linear loads affect the sinusoidal output voltage of inverters, as they increase the total harmonic distortion (THD), resulting in the difficulty of meeting IEEE standard 1547 [1–4]. In order to regulate the output voltage in the presence of uncertain load conditions, a robust controller with good transient and dynamic response is required [5].

Conventionally, PWM-based controllers are small-signal model dependent; therefore, practically, the inverter state-space equations do not remain the same because the states of the switches change very rapidly during wide operating conditions. Moreover, the modeling of the discontinuous control variable as a continuous function, called the duty ratio, further complicates the problem, hence, the mathematical model will only work when operating very near the prescribed equilibrium point [6,7].

In order to achieve wide range operations, researchers have proposed different types of non-linear control techniques [8–11]. Out of these, sliding mode (SM) control is well known

for being robust and parameter-invariant [12–15]. SMC for power inverters achieves the desired output voltage regulation in a wide range of operating conditions [16–18]. Power inverters are inherently compatible with the SMC technique, due to their discrete switching nature and being a variable structure system [19,20]. SMC has some unique features, such as robustness, order reduction, stability and precise regulation [21,22]. Moreover, the average model of the power converter is not essential for SMC [23,24].

Ideally, SMC operates at an infinite switching frequency. However, an infinite switching frequency is not achievable in practical systems. Hence, the switching frequency must be kept in a practical range. In [25,26], an adaptive feedforward-based hysteresis controller is presented to select the specific range of switching frequency. In the case of variations, the hysteresis region of the SMC changes with respect to any disturbances in the load [27]. These schemes achieve a finite but variable frequency, downgrading the power quality and resulting in increased electromagnetic interference (EMI).

In recent studies, many control techniques have been proposed to address the aforementioned problem of the frequency drifts in SMC. In [28], adaptive hysteresis controller is utilized to achieve a fixed frequency SM controller by varying the hysteresis band. In this method, additional sensors are required to gather the information of system states, which increases its complexity and cost.

The zero average dynamics (ZAD) technique is also reported in the context of fixed switching frequency. This technique changes the duty cycle of the power switch in a controlled manner to ensure the zero T-periodic average of the discontinuous function. This method achieves a fixed frequency operation and is practically demonstrated by the authors [29]. Major drawbacks of this technique are the complex computations and the requirement of high-speed and expensive processors.

In [30], a fixed frequency SMC is proposed, where the discontinuous sign function is replaced by the smoothed control law within the specific boundary limits. This achieves the fixed switching frequency by PWM implementation of this control law. However, the disturbance rejection properties of this controller are lost within this boundary layer. PWM SMC is also reported in [31,32], where the equivalent control law is produced from the measured states of the system rather than from the discontinuous function, which compromises the inherent properties of SMC. Moreover, this method also requires more components as compared to a hysteresis modulator. For better understanding, a comparison of variable and fix-frequency SMC is represented in Table 1.

By and large, all of the prevalent fixed switching frequency-based SMC are either too complex or result in a loss of parametric variance, thereby compromising the robustness and disturbance rejection properties of the feedback system. Hence, a fixed frequency SMC is needed for the power inverter application, which offers ease of implementation by virtue of using off-the-shelf and low-cost components, while retaining the inherent advantages of SMC.

In this research, a SMC based upon the filter extraction of equivalent control from the discontinuous sign function is proposed to achieve the fixed switching frequency along with reducing the implementation cost and complexity. It is worth mentioning that the discontinuous control law generated from the sign function cannot be applied directly to multi-level and unipolar converters. In this regard, the proposed technique also provides a mechanism for generating a multi-switch converter sequence along with reducing the switching losses. Furthermore, in the current era of industrialization, robust fixed-frequency controllers for power electronic converters are a fundamental requirement because they find applications in advanced automotive power systems, regulated power supplies, heating furnaces, and modern electronic equipment, which necessitates the use of grid-connected energy storage systems as well.

The organization of this paper is as follows: The proposed technique along with the PWM-based hysteresis sliding mode control technique are presented in Section 2. Results and comparison of the controllers are discussed in Section 3. The conclusion and future work are presented in Section 4.

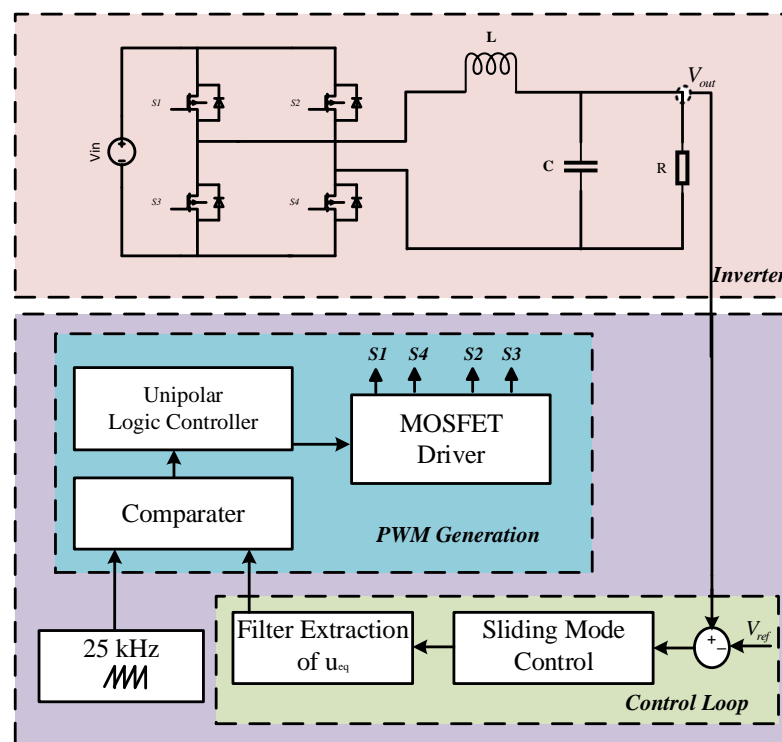
**Table 1.** Advantages and disadvantages of variable- and fixed-frequency SMC.

Controller	Advantage	Disadvantage
Variable-frequency SMC	<ul style="list-style-type: none"> <li>• It is completely parameter invariant.</li> <li>• Relatively simpler hardware implementation</li> <li>• Operates at a limited frequency, which is practical.</li> </ul>	<ul style="list-style-type: none"> <li>• It cannot be utilized in power electronic converters and inverters because the frequency is not fixed.</li> <li>• It cannot be used in applications where frequency components, such as capacitors and inductors, are used.</li> </ul>
Fixed-frequency SMC	<ul style="list-style-type: none"> <li>• Operating at a set frequency,</li> <li>• They can be used with power electronic converters and inverters.</li> <li>• They are especially useful in applications where the frequency dependent components such as capacitors and inductors are employed.</li> </ul>	<ul style="list-style-type: none"> <li>• Some methods of regulating the frequency put the robustness of the system at risk.</li> <li>• Additional hardware is incorporated into the overall design.</li> </ul>

## 2. Methods

### 2.1. Proposed Technique

The bipolar PWM technique produces more harmonic content and switching losses in an inverter as compared to the unipolar PWM switching method [33,34]. Therefore, the unipolar PWM technique is selected for the inverter, due to its better performance in terms of THD and efficiency [35]. Applying the circuit analysis technique to the unipolar inverter shown in Figure 1, we obtain the following equation:

**Figure 1.** Block diagram representation of proposed SM controller.

$$V_{out} = uV_{in} - L \frac{di_L}{dt} \quad (1)$$

where  $u$  is the control input,  $u \in \{1, 0, -1\}$ , and representing  $V_{out}$  as the output voltage, we obtain the following:

$$i_C = i_L - i_o \quad (2)$$

The capacitor current can be written as follows:

$$i_C = C \frac{dV_{out}}{dt} \quad (3)$$

Rearranging Equation (2) and using  $i_C$  from Equation (3), we obtain the following:

$$i_L = C \frac{dV_{out}}{dt} + i_o \quad (4)$$

where  $i_o$  is the load current and mathematically given as follows:

$$i_o = \frac{V_{out}}{R} \quad (5)$$

Here,  $i_C$  and  $i_L$  represent the capacitor and inductor current, respectively. By substituting Equation (4) into (1) and after some mathematical manipulation, we obtain the following:

$$\dot{V}_{out} = \frac{uV_{in}}{LC} - \frac{V_{out}}{LC} - \frac{\dot{V}_{out}}{RC} \quad (6)$$

Consider the error between the output voltage and reference voltage and its derivative as state variables  $x_1$  and  $x_2$ , represented mathematically as follows:

$$x_1 = V_{out} - V_{ref} \quad (7)$$

$$x_2 = \dot{x}_1 = \dot{V}_{out} - \dot{V}_{ref} \quad (8)$$

Differentiating Equation (8) and substituting the value of  $V_{out}$  from Equation (6), we obtain variable  $x_2$ :

$$\dot{x}_2 = \frac{uV_{in}}{LC} - \frac{V_{out}}{LC} - \frac{\dot{V}_{out}}{RC} - \ddot{V}_{ref} \quad (9)$$

To represent Equation (9) in terms of state variables  $x_1$  and  $x_2$ , we modify it by adding and subtracting  $\frac{V_{ref}}{LC}$  and  $\frac{\dot{V}_{ref}}{RC}$ :

$$\dot{x}_2 = -\frac{1}{LC}x_1 - \frac{1}{RC}x_2 + \frac{uV_{in}}{LC} - \frac{1}{LC}V_{ref} - \frac{1}{RC}\dot{V}_{ref} - \ddot{V}_{ref} \quad (10)$$

We select the sliding surface  $\zeta$  as follows:

$$\zeta(x) = \alpha x_1 + x_2 = 0; \text{ \& } \alpha > 0 \quad (11)$$

where  $\alpha$  is the controller gain. By differentiating Equation (11), we obtain the following:

$$\dot{\zeta} = \alpha x_2 + \dot{x}_2 = 0 \quad (12)$$

By using Equations (10) and (12), we obtain the following:

$$\dot{\zeta} = -\frac{1}{LC}x_1 - \frac{1}{RC}x_2 + \alpha x_2 + \frac{uV_{in}}{LC} - \frac{1}{LC}V_{ref} - \frac{1}{RC}\dot{V}_{ref} - \ddot{V}_{ref} = 0 \quad (13)$$

Solving Equation (13) for the equivalent control, we obtain the following:

$$u_{eq} = \frac{LC}{V_{in}} \left( \frac{1}{LC}x_1 - \frac{\alpha}{RC}x_1 + \alpha^2 x_1 + \frac{1}{LC}V_{ref} + \frac{1}{RC}\dot{V}_{ref} - \ddot{V}_{ref} \right) \quad (14)$$

if  $w(t) = \frac{1}{LC}V_{ref} + \frac{1}{RC}\dot{V}_{ref} - \ddot{V}_{ref}$ , it can also be written as follows:

$$u_{eq} = \frac{LC}{V_{in}} \left( \left( \frac{1}{LC} - \frac{\alpha}{RC} + \alpha^2 \right) x_1 + w(t) \right) \quad (15)$$

### 2.1.1. Filter Extraction

Ideally, the operating frequency of an SM controller is infinite; however, the infinite switching frequency is not achievable in practical systems, due to the physical constraints. It causes oscillations of the state variables in the neighborhood of the sliding surface  $\varsigma = 0$ . These oscillations are a combination of low and high frequency components. The low frequency part of these oscillations is responsible for the motion on the sliding surface, and can be filtered out using a low pass filter [36,37]. Therefore, a low pass filter is designed by selecting an appropriate time constant  $\tau$  such that it passes the low frequency component without distortion, thereby eliminating the high-frequency component. We propose a first-order RC filter with time constant  $\tau = R_1C_1$ , where  $R_1$  is the resistance and  $C_1$  is the capacitance of the filter. By using Kirchoff's voltage law, the mathematical expression of control input  $u$  against the filter output  $f(t)$  is obtained as follows:

$$u = R_1i(t) + f(t) \quad (16)$$

where  $i(t)$  is the current through the filter given by  $i(t) = C_1 \frac{d}{dt}f(t)$ :

$$u = R_1C_1 \frac{d}{dt}f(t) + f(t) \quad (17)$$

$$u = \tau \frac{d}{dt}f(t) + f(t) \quad (18)$$

Under the assumption of the infinite switching frequency and a very small time constant of the low pass filter, the output of the filter  $f(t)$  will approach the equivalent control of the system, given as follows:

$$\lim_{f_s \rightarrow \infty, \tau \rightarrow 0} f(t) = u_{eq} \quad (19)$$

where  $f_s$  is the switching frequency under these ideal conditions; the width,  $\delta$ , in which the states oscillate, approaches 0, and the motion of the SM controller is closer to the ideal one. Physically, for the extraction of the equivalent control, the following condition must be satisfied:

$$f_s \gg \frac{1}{\tau} \quad (20)$$

It must be pointed out that the filter extracted equivalent control carries the information and disturbances faced by the system. As illustrated in Figure 1, after extracting  $u_{eq}$ , the control signal  $V_c$  is PWM implemented, using the ramp carrier signal with peak amplitude  $V_p$  and switching frequency  $f_s$ . For stable operation, the peak amplitude of the carrier signal  $V_p$  must be higher than the amplitude of control signal  $V_c$  [38].

### 2.1.2. Existence of the SM

In this research, to fulfill the condition  $V_p > V_c$  for stable switching operation, the voltage limiter circuit is realized using the Zener diode. It is important to note that the obtained PWM switching signal will result in a fixed-frequency SM operation. We take a positive definite Lyapunov function as follows:

$$V(x, t) = \frac{1}{2}\zeta^2 \quad (21)$$

According to the Lyapunov theory, for the stable operation of the system,  $\dot{V}(x, t)$  shall be less than 0 at any time after  $t = 0$ . By differentiating Equation (21), we obtain the following:

$$\dot{V}(x, t) = \zeta\dot{\zeta} \quad (22)$$

Substituting the value of  $\dot{\zeta}$  from (13) into Equation (22) results in the following:

$$\dot{V}(x, t) = \zeta \left[ -\frac{1}{LC}x_1 - \frac{1}{RC}x_2 - \alpha^2x_1 + \frac{uV_{in}}{LC} - \frac{1}{LC}V_{ref} - \frac{1}{RC}\dot{V}_{ref} - \ddot{V}_{ref} \right] \quad (23)$$

Considering  $u = -\text{sign}(\zeta)$  and substituting in Equation (23), we obtain the following:

$$\dot{V}(x, t) = \zeta \left[ -\frac{1}{LC}x_1 - \frac{1}{RC}x_2 - \alpha^2x_1 - \frac{V_{in}}{LC}\text{sign}(\zeta) - \frac{1}{LC}V_{ref} - \frac{1}{RC}\dot{V}_{ref} - \ddot{V}_{ref} \right] \quad (24)$$

If  $\zeta > 0$ , it can be seen simply from Equation (24) that  $\dot{\zeta}$  is negative definite. Hence, it satisfies the stability of the sliding manifold at  $\zeta = 0$ . To ensure the sliding condition, we must be satisfy in the equation the following condition:

$$V_{in} > I_L \left( \frac{L}{RC} - \frac{\alpha}{C} \right) + V_{out} \left( 1 + \frac{\alpha}{RC} - \frac{L}{R^2C} \right) \quad (25)$$

where  $\alpha$  must satisfy the following:

$$\alpha \left( \alpha - \frac{1}{RC} \right) > -\frac{1}{LC} \quad (26)$$

## 2.2. PWM Based Hysteresis Sliding Mode Control

In order to compare the results of the proposed controller, a PWM-based hysteresis SM controller is also implemented. For the better understanding of the reader, the design of this controller is also presented. Taking the error,  $e$ , of the inverter as the system state, we define the following:

$$e = V_{ref} - V_{out} \quad (27)$$

where  $V_{ref}$  is the reference voltage and  $V_{out}$  is the output voltage of the inverter. Identifying  $\frac{d}{dt}V_{out} = \frac{I_C}{C}$  and substituting it in Equation (8), we obtain the following:

$$\ddot{x}_1 = \frac{V_{out}}{LC} - \frac{\tilde{u} \times V_{in}}{LC} + \frac{I_C}{RC^2} \quad (28)$$

As discussed earlier, SM control cannot be applied directly to the inverter. So the PWM-modulated smoothed control law is utilized for practical implementation and achieves a fixed-frequency SM control. A boundary layer of width  $\delta$  is introduced to reduce the chattering problem in the neighborhood of the sliding surface [30]. The control law is smoothed in a narrow boundary layer instead of the discontinuous control law. It shall be noticed that the increase in the length  $\delta$  will also increase the tracking error, and as a result, the robustness will be compromised within this region. The PWM slope of the carrier signal must be higher than that of the input signal. In [30], the slope of the carrier is given as follows:

$$S_c = 4V_p \times f_s \quad (29)$$

where  $V_p$  and  $f_s$  are the amplitude and frequency of the carrier signal, respectively. The sliding surface is defined as follows:

$$\zeta(x) = \beta x_1 + x_2 = 0 \quad (30)$$

By using the sliding surface model, it is clear that the input control law to the PWM consists of two terms, namely, the capacitor current error and output voltage error:

$$\frac{\zeta(x)}{\delta} = \frac{1}{\delta C}(I_r - I_C) + \frac{\beta}{\delta}(V_r - V_o) \quad (31)$$

A sinusoidal waveform is obtained at the output of the inverter in a steady state condition, and the output voltage error always approaches zero. In (31),  $\frac{1}{\delta C}(I_r - I_C) \gg \frac{\beta}{\delta}(V_r - V_o)$ , so it simplifies to the following:

$$\frac{\zeta(x)}{\delta} = \frac{1}{\delta C}(I_r - I_C) = \frac{I_{ripple}}{\delta C} \quad (32)$$

where  $I_{ripple} = I_r - I_C$ . It shall be noticed that the capacitor current contains noise signals with abrupt changes; therefore, the value of  $\delta$  is selected to compensate for this effect. Moreover, it can be seen in Figure 2 that the capacitor and inductor are in series, hence, the ripple error current is the same for both the capacitor and inductor and is represented in the following: (33),

$$I_{ripple} = KT \left( \frac{V_{in} - V_o}{L \times f_s} \right) \quad (33)$$

and

$$K = m \times \sin(2\pi f_o t) \quad (34)$$

where  $K$ ,  $T$ ,  $m$  and  $f_o$  represent the duty ratio, time period of the carrier signal, modulation factor and output frequency. Substituting (33) and (34) into (32) and then deriving for  $T$ , the slope of input signal is obtained as the following:

$$S_i = \frac{V_{in}}{4LC\delta} \quad (35)$$

For limitation, the PWM slope of the carrier should be greater than the slope of the input signal, as follows:

$$S_c > S_i \quad (36)$$

Now, the value of  $\delta$  can be found by substituting Equations (29) and (35) into (36) as follows:

$$4V_m \times f_s \gg \frac{V_{in}}{4LC\delta} \quad (37)$$

which gives the following:

$$\delta \gg \frac{V_{in}}{16LCV_m f_s} \quad (38)$$

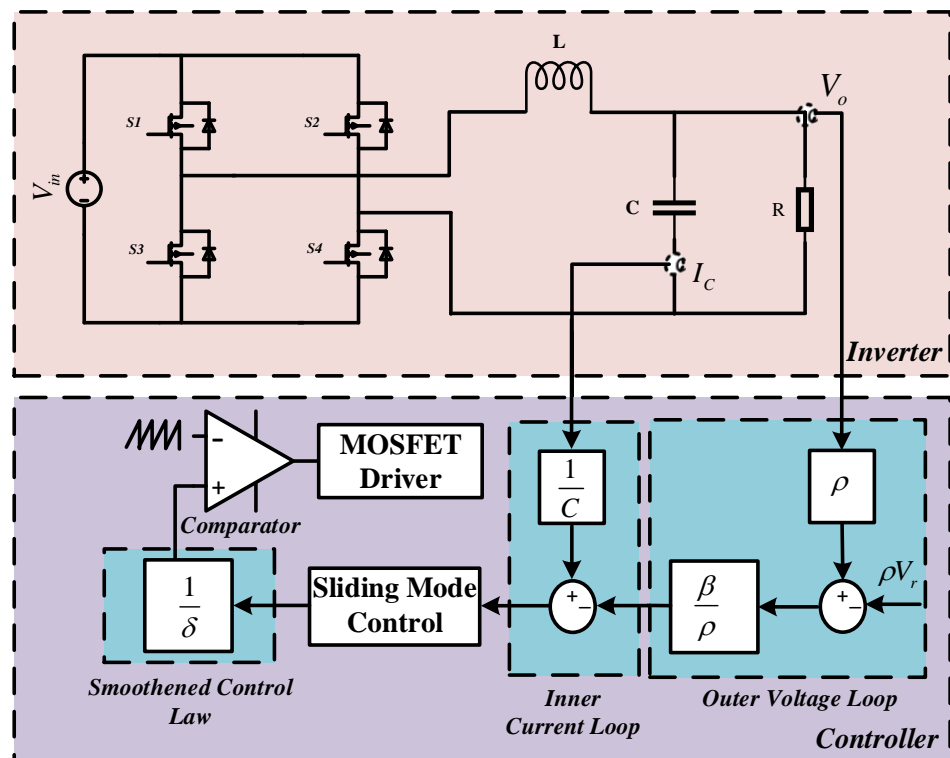


Figure 2. Block diagram representation of PWM-based hysteresis sliding mode control.

### 2.3. Controller Implementation

To examine the performance of the proposed controller, it is simulated and implemented in hardware as well. The Simulink tool of MATLAB-2017a is used to simulate the proposed controller and PWM-based hysteresis SM controller for the inverter. The simulated parameters of the inverter are provided in Table 2 in which  $f_s$  and  $F$  are the switching frequency and power frequency of the inverter, respectively. In the Simulink model, the configuration parameters are selected such that *ode3(Bogacki-shampine)* is a solver with the fixed step size of  $10^{-6}$  s.

The controller is also implemented experimentally. The parameters of the inverter are provided in Table 3. The H-Bridge inverter consists of four power MOSFET IRF3205 with 8 mΩ ultra low on-resistance and 110 A maximum current capability. The output filter of the inverter consists of a capacitor made with two series 4.7 μF, 25 V capacitors and an inductor of 1.5 mH constructed with a ferrite core. The operating frequency of the inverter is selected to be 25 kHz. There is a compromise in selecting the switching frequency, as its increased value increases the switching losses, whereas a low switching frequency results in higher magnitude of the chattering signals. A 50 Hz square wave is generated from an FPGA. The FPGA development board is powered through the USB port of the laptop, which is not connected to the mains, to provide isolation.

**Table 2.** Simulated parameters of inverter.

Description	Symbol	Value
Input Voltage	$V_{DC}$	350 V
Output Voltage	$V_{out}$	220 Vrms
Switching Frequency	$f_s$	25 kHz
Power Frequency	$F$	50 Hz
Inductance	$L$	860 $\mu$ H
Capacitance	$C$	10 $\mu$ F
Load Resistance	$R_{Load}$	16–100 $\Omega$

**Table 3.** Experimental parameters of inverter.

Description	Symbol	Value
Input Voltage	$V_{DC}$	18 V
Output Voltage	$V_{out}$	12 Vrms
Switching Frequency	$f_s$	25 kHz
Power Frequency	$F$	50 Hz
Inductance	$L$	1.4 mH
Capacitance	$C$	2.3 $\mu$ F
Load Resistance	$R_{Load}$	10–100 $\Omega$

A gate driver circuit consisting of two IR2110 ICs is used to drive the high and low side of the IR3205 present at each leg of the H-Bridge. In order to operate at higher frequencies, it is observed experimentally that the diode in the bootstrap circuitry of the gate driver should have a fast reverse recovery time of less than 40 ns. If the diode reverse recovery time is higher than this value, then it will not be able to apply the next switching pulse, as it will take more time to return to the original state. Therefore, the FR106 diode with a reverse recovery time of 250 ns is used in this circuit. All the experimental results presented in this thesis were obtained using the 70 MHz Rigol oscilloscope with the sampling rate of 1 G samp/s. The experimental setup to validate the performance of the proposed controller is shown in Figure 3.

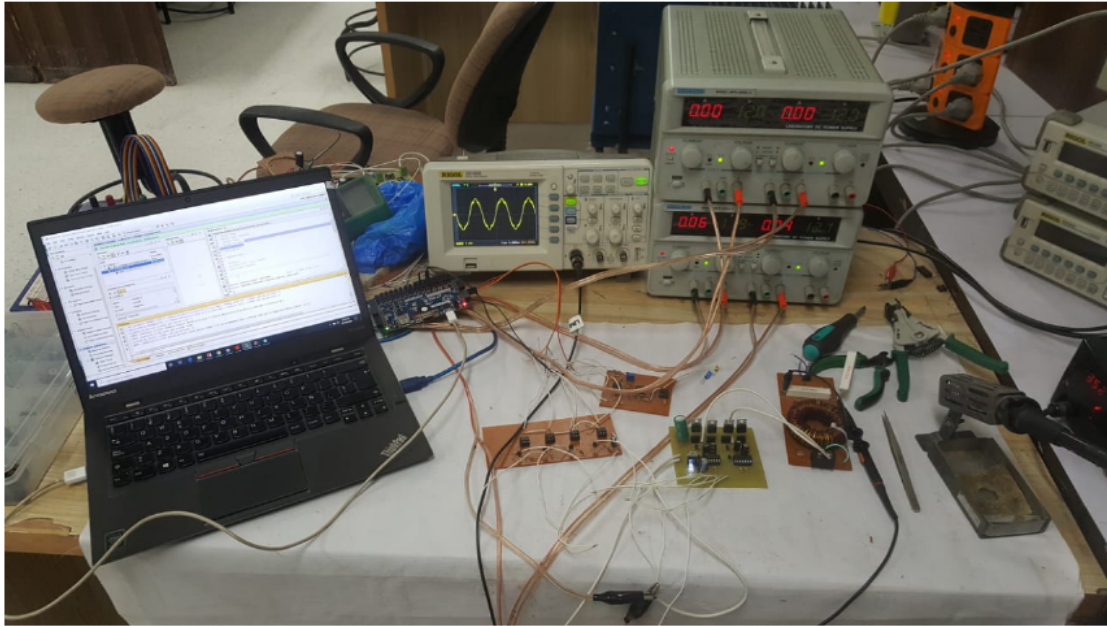


Figure 3. Experimental setup of the proposed technique.

### 3. Results and Discussion

To examine the performance of the controller, both simulation results and hardware implemented outputs are presented. Figure 4a shows the output voltage and current of the inverter at maximum load with a total harmonic distortion (THD) of 0.7%. The gate signals obtained from the proposed controller to operate power switches are presented in Figure 4b. The simulation results show that both the controllers have zero steady-state error and achieve the desired 220 Vrms. It should be noted that the proposed technique achieves zero steady-state error without having an extra current loop and resonance compensator. This establishes the cost effectiveness and simplicity of the proposed control technique.

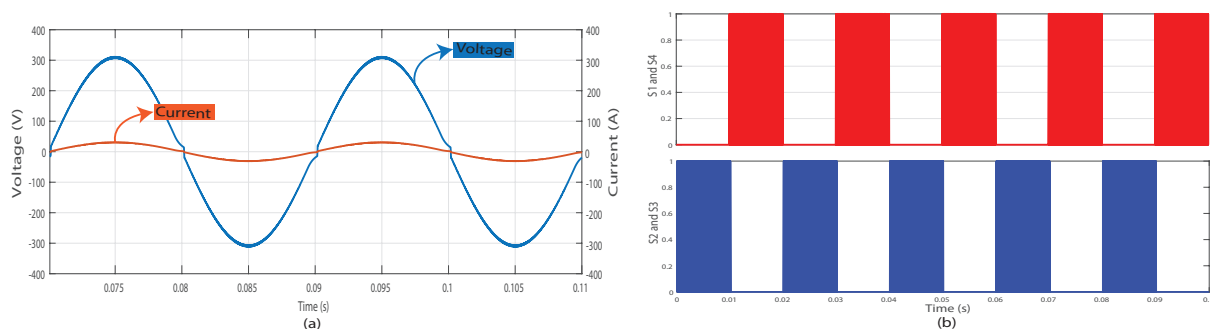
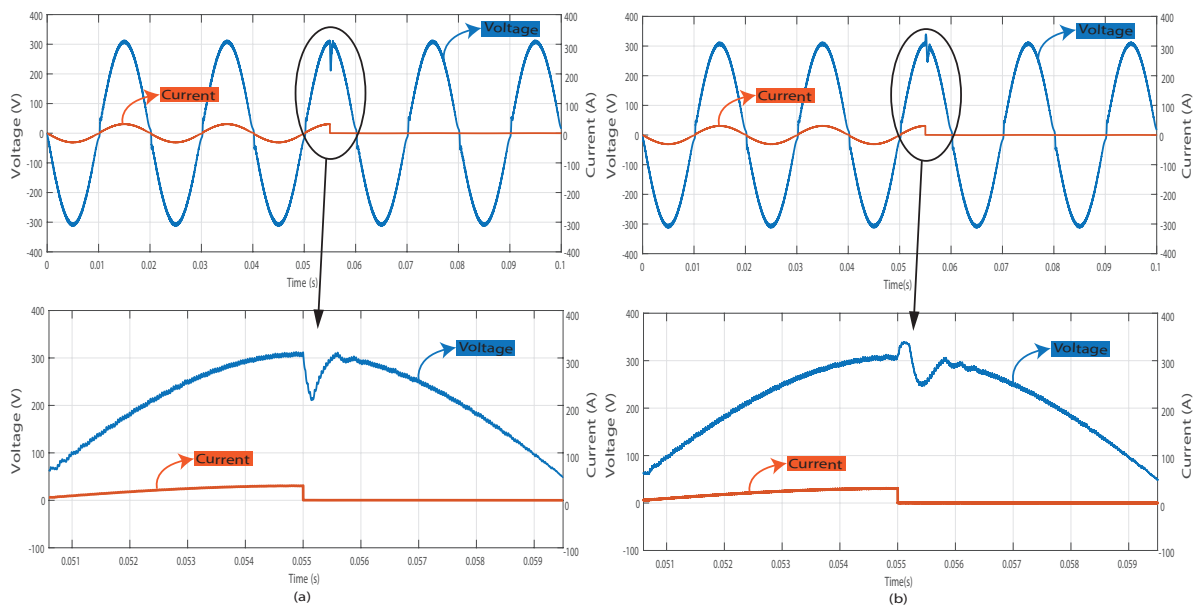


Figure 4. Waveforms of the simulation results. (a) Output voltage and current of unipolar power inverter. (b) Switching signals of inverter with 180 degree phase shift.

Simulation results for step load conditions of PWM-based hysteresis SM controller is shown in Figure 5. This controller gives 31% undershoot and recovers in 0.6 ms. The overshoot by disconnecting the existing full load is also 12% of the rated voltage, and it settles down in 0.8 ms.



**Figure 5.** Simulation results of the PWM-based hysteresis SM controller. (a) Transient response of the system when additional load is connected. (b) Transient response of the system when additional load is removed.

Figure 6 represents the step load conditions of the proposed controller. This controller shows an improvement of 37% by reducing the undershoot to 18.5% and shows 50% improvement in the transient time by recovering in 0.3 ms. It exhibits an improvement of 42% by reducing the overshoot to 7% and improves the recovery time by 50% by settling in 0.4 ms. The overall proposed control technique exhibits robust performance as compared to the PWM-based hysteresis SM controller. The quantification results of both techniques are compared in Table 4. The input voltage variation of the proposed controller is presented in Table 5.

**Table 4.** Comparison of the simulation results.

Approaches	Transient Time	Overshoot	Undershoot
PWM Based Hysteresis SMC	0.6 ms	12%	31%
Proposed Technique	0.3 ms	7%	18.5%

**Table 5.** Input Voltage Variation.

Input Voltage ( $V_{DC}$ )	Output Voltage ( $V_{rms}$ )
350	220.47
340	220.34
330	220.11
320	219.98
310	219.56
300	219.31

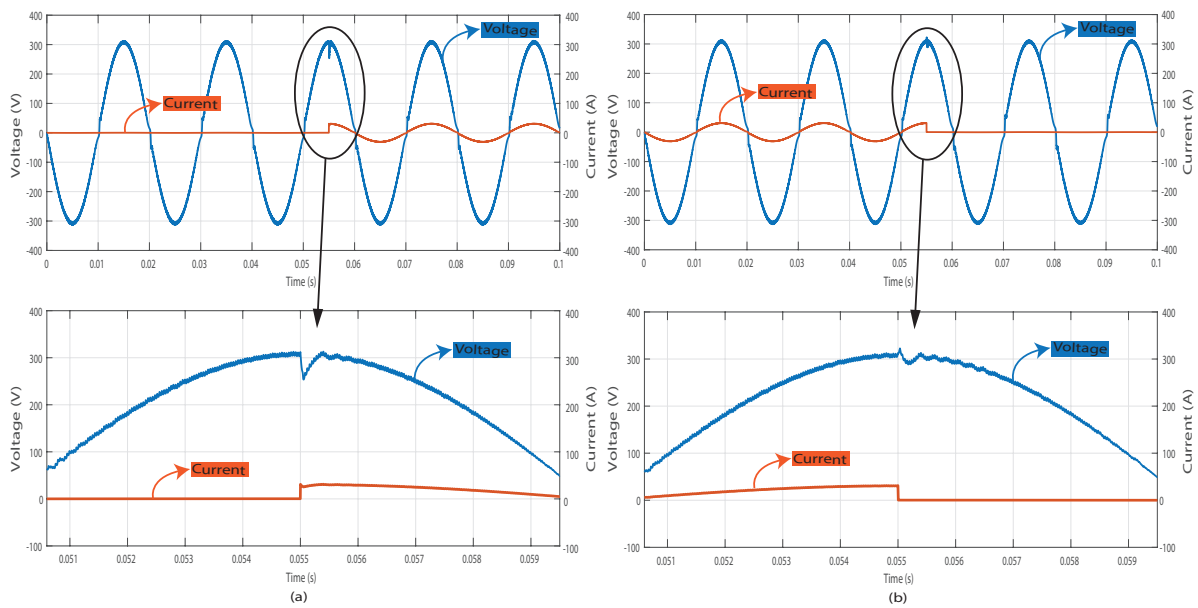


**Figure 6.** Simulation based SM controller. (a) Transient response of the system when additional load is connected. (b) Transient response of the system when additional load is removed.

In Figure 7, the transient response of the inverter is presented at the same voltage level for both the simulation and hardware, which validates the performance of the controller and in Figure 8a, a FFT analysis of the output voltage is presented. This waveform shows that there is only a fundamental frequency component with no other prominent harmonic component. The calculated THD of the output voltage is less than 0.8%. Figure 8b shows that the transient time of the output voltage in the step load condition is less than 1 ms. Figure 8c shows the output voltage and current of the inverter at a linear load. The proposed controller also satisfies the zero steady-state error. Figure 8d represents the gating signal for the inverter, which is obtained from the controller. So, the proposed controller implemented experimentally also shows good performance.

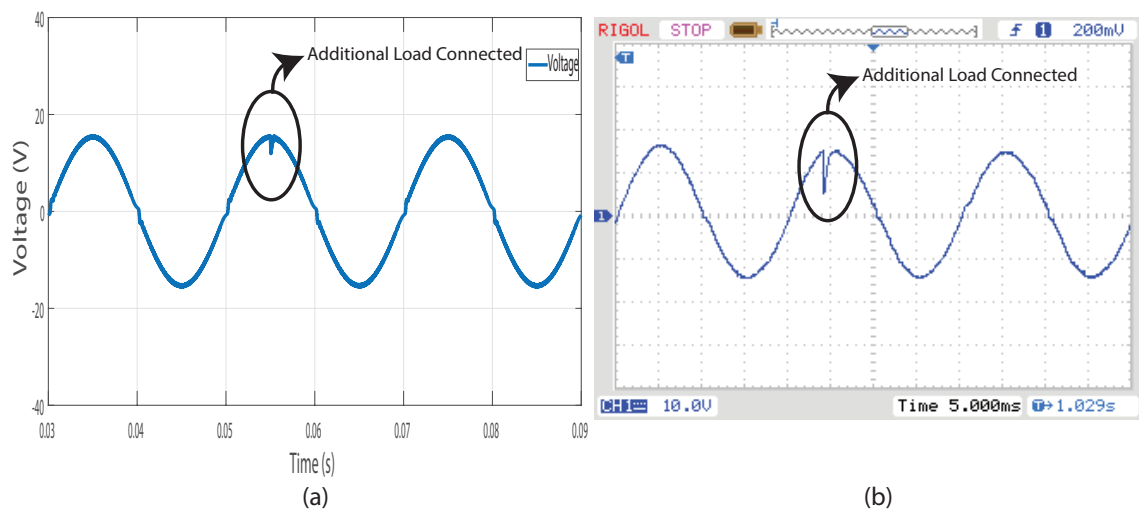


**Figure 7.** Transient response of the system when the additional load is connected. (a) Simulation result. (b) Hardware result.

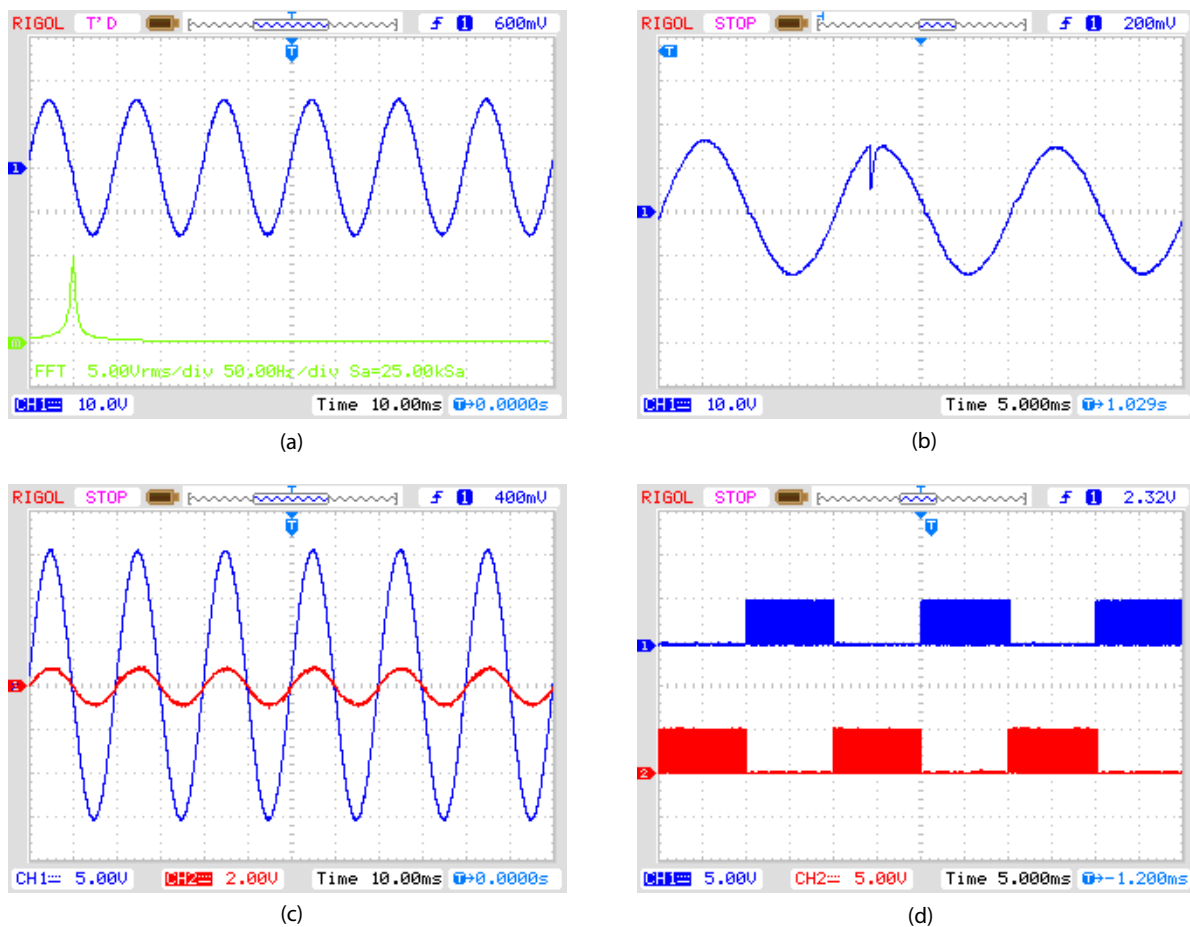


**Figure 8.** Waveforms of the experimental results. (a) FFT analysis of output voltage (b) Transient response of output voltage indicating robustness when load is shifted from 100 Ω to 9.1 Ω. (c) Output voltage and current of inverter. (d) Switching signals for gate driver to operate inverter in a closed-loop system.

#### 4. Conclusions

Discontinuous function shows robustness and disturbance rejection to unmodeled dynamics; however, practically, this causes frequency drifts. The proposed SM controller achieves a fixed-switching frequency by using the filter extraction of the equivalent control. The model is implemented on a power inverter and the results are compared with a PWM-SM controller to validate the effectiveness of the presented controller. Zero steady-state error and better transient response are exhibited by the proposed technique, as it shows 50% improvement in settling time. Moreover, it improves the voltage undershoot and overshoot by 37% and 42%, respectively. Hence, the proposed SM controller demonstrates robustness and parameter invariance, due to the direct implementation of the discontinuous function.

Some of the future prospects arising from the presented work are discussed here as well. Inverters are the essential part of the regenerative braking units of hybrid electric vehicles. The proposed SMC technique may be explored for this system to improve the transient response and robustness. This technique can be evaluated based on the economy and efficiency of the produced energy. One of the possible directions for future work is to utilize this proposed technique on the inverter, along with the MPPT algorithm applied to the boost converter, to obtain cheap, transformer-less and efficient energy, along with a compact system from PVs.

**Author Contributions:** A.R.Y. provided the conceptualization and supervised the project. M.A., M.R., B.S., S.Z. and A.Y. developed the methodology for the investigation and performed formal analysis. All authors have read and agreed to the published version of the manuscript.

**Funding:** This research received no external funding.

**Acknowledgments:** The authors would like to thank the University of Lahore.

**Conflicts of Interest:** The authors declare no conflict of interest.

## References

1. Ali, M.; Aamir, M.; Khan, H.S.; Waqar, A.; Haroon, F.; Jafri, A.R. Lyapunov Stability and Performance Analysis of the Fractional Order Sliding Mode Control for a Parallel Connected UPS System under Unbalanced and Nonlinear Load Conditions. *Energies* **2018**, *11*, 3475. [[CrossRef](#)]
2. Anand, V.; Singh, V. Implementation of cascaded asymmetrical multilevel inverter for renewable energy integration. *Int. J. Circuit Theory Appl.* **2021**, *49*, 1776–1794. [[CrossRef](#)]
3. Turksroy, A.; Hames, Y.; Teke, A.; Latran, M.B. A novel adaptive switching method to reduce DC-Link capacitor ripple in PV based grid-connected inverter. *Sol. Energy* **2018**, *173*, 702–714. [[CrossRef](#)]
4. Carballo, R.E.; Botterón, F.; Oggier, G.G.; García, G.O. Multiple resonant controllers strategy to achieve fault ride-through and high performance output voltage in UPS applications. *IET Power Electron.* **2018**, *11*, 2415–2426. [[CrossRef](#)]
5. Xu, D.; Wang, G.; Yan, W.; Yan, X. A novel adaptive command-filtered backstepping sliding mode control for PV grid-connected system with energy storage. *Sol. Energy* **2019**, *178*, 222–230. [[CrossRef](#)]
6. Middlebrook, R. Small-signal modeling of pulse-width modulated switched-mode power converters. *Proc. IEEE* **1988**, *76*, 343–354. [[CrossRef](#)]
7. Lee, B.K.; Ehsami, M. A simplified functional simulation model for three-phase voltage-source inverter using switching function concept. *IEEE Trans. Ind. Electron.* **2001**, *48*, 309–321.
8. Ahmad, A.; Ullah, N.; Ahmed, N.; Ibeas, A.; Mehdi, G.; Herrera, J.; Ali, A. Robust control of grid-tied parallel inverters using nonlinear backstepping approach. *IEEE Access* **2018**, *7*, 111982–111992. [[CrossRef](#)]
9. Naji Alhasnawi, B.; Jasim, B.H.; Anvari-Moghaddam, A.; Blaabjerg, F. A New Robust Control Strategy for Parallel Operated Inverters in Green Energy Applications. *Energies* **2020**, *13*, 3480. [[CrossRef](#)]
10. Safa, A.; Berkouk, E.M.; Messlem, Y.; Gouichiche, A. A robust control algorithm for a multifunctional grid tied inverter to enhance the power quality of a microgrid under unbalanced conditions. *Int. J. Electr. Power Energy Syst.* **2018**, *100*, 253–264. [[CrossRef](#)]
11. Amirkhan, S.; Radmehr, M.; Rezaejanad, M.; Khormali, S. A robust control technique for stable operation of a DC/AC hybrid microgrid under parameters and loads variations. *Int. J. Electr. Power Energy Syst.* **2020**, *117*, 105659. [[CrossRef](#)]
12. Alsmadi, Y.M.; Chairez, I.; Utkin, V. Sliding mode control of an ozone generator based on dual AC/DC/AC power converters. *Proc. Inst. Mech. Eng. Part I J. Syst. Control Eng.* **2021**, *235*, 448–460. [[CrossRef](#)]
13. Alsmadi, Y.M.; Utkin, V.; Haj-Ahmed, M.; Xu, L.; Abdelaziz, A.Y. Sliding-mode control of power converters: AC/DC converters & DC/AC inverters. *Int. J. Control* **2018**, *91*, 2573–2587.
14. Tian, Z.; Lyu, Z.; Yuan, J.; Wang, C. UDE-based sliding mode control of DC–DC power converters with uncertainties. *Control Eng. Pract.* **2019**, *83*, 116–128. [[CrossRef](#)]
15. Utkin, V.; Guldner, J.; Shijun, M. *Sliding Mode Control in Electro-Mechanical Systems*; CRC Press: Boca Raton, FL, USA, 1999; Volume 34.
16. Sudalaimani, M.; Revathi, L.; Senthilkumar, N. Direct Power based Sliding Mode Control of AC-DC Converter with Reduced THD. *Teh. Vjesn.* **2018**, *25*, 72–79.
17. Hu, J.; Shang, L.; He, Y.; Zhu, Z. Direct active and reactive power regulation of grid-connected DC/AC converters using sliding mode control approach. *IEEE Trans. Power Electron.* **2011**, *26*, 210–222. [[CrossRef](#)]
18. Wanjekeche, T. Modeling, control and experimental investigation of a cascaded hybrid modular inverter for grid interface application. *IEEE Access* **2018**, *6*, 21296–21313. [[CrossRef](#)]
19. Han, J.S.; Kim, T.I.; Oh, T.H.; Lee, S.H. Effective disturbance compensation method under control saturation in discrete-time sliding mode control. *IEEE Trans. Ind. Electron.* **2019**, *67*, 5696–5707. [[CrossRef](#)]
20. Homaeinezhad, M.; Yaqubi, S. Discrete-time sliding-surface based control of parametrically uncertain nonlinear systems with unknown time-delay and inaccessible switching mode detection. *Int. J. Control* **2019**, *94*, 1–20. [[CrossRef](#)]
21. Repecho, V.; Sierra-González, A.; Ibarra, E.; Biel, D.; Arias, A. Enhanced DC-link voltage utilization for sliding mode controlled PMSM drives. *IEEE J. Emerg. Sel. Top. Power Electron.* **2020**, *9*, 2850–2857. [[CrossRef](#)]
22. Alam, W.; Ahmad, S.; Mehmood, A.; Iqbal, J. Robust sliding mode control for flexible joint robotic manipulator via disturbance observer. *Interdiscip. Descr. Complex Syst. INDECS* **2019**, *17*, 85–97. [[CrossRef](#)]
23. Yasin, A.R.; Ashraf, M.; Bhatti, A.I.; Uppal, A.A. Fixed frequency sliding mode control of renewable energy resources in DC micro grid. *Asian J. Control* **2019**, *21*, 2074–2086. [[CrossRef](#)]
24. Chen, Y.; Fei, J. Dynamic Sliding Mode Control of Active Power Filter With Integral Switching Gain. *IEEE Access* **2019**, *7*, 21635–21644. [[CrossRef](#)]
25. Tan, S.C.; Lai, Y.; Tse, C.K.; Cheung, M.K. Adaptive feedforward and feedback control schemes for sliding mode controlled power converters. *IEEE Trans. Power Electron.* **2006**, *21*, 182–192.
26. Repecho, V.; Biel, D.; Olm, J.M.; Colet, E.F. Switching frequency regulation in sliding mode control by a hysteresis band controller. *IEEE Trans. Power Electron.* **2016**, *32*, 1557–1569. [[CrossRef](#)]

27. Abrishamifar, A.; Ahmad, A.; Mohamadian, M. Fixed Switching Frequency Sliding Mode Control for Single-Phase Unipolar Inverters. *IEEE Trans. Power Electron.* **2012**, *27*, 2507–2514. [[CrossRef](#)]
28. Holmes, D.G.; Davoodnezhad, R.; McGrath, B.P. An improved three-phase variable-band hysteresis current regulator. *IEEE Trans. Power Electron.* **2012**, *28*, 441–450. [[CrossRef](#)]
29. Ramos, R.R.; Biel, D.; Fossas, E.; Guinjoan, F. A fixed-frequency quasi-sliding control algorithm: Application to power inverters design by means of FPGA implementation. *IEEE Trans. Power Electron.* **2003**, *18*, 344–355. [[CrossRef](#)]
30. Abrishamifar, A.; Ahmad, A.A.; Elahian, S. Fixed frequency sliding mode controller for the buck converter. In Proceedings of the 2011 2nd Power Electronics, Drive Systems and Technologies Conference, Tehran, Iran, 16–17 February 2011; pp. 557–561.
31. Yasin, A.R.; Ashraf, M.; Bhatti, A.I. Fixed frequency sliding mode control of power converters for improved dynamic response in DC micro-grids. *Energies* **2018**, *11*, 2799. [[CrossRef](#)]
32. Jazi, H.N.; Goudarzian, A.; Pourbagher, R.; Derakhshandeh, S.Y. PI and PWM sliding mode control of POESLL converter. *IEEE Trans. Aerosp. Electron. Syst.* **2017**, *53*, 2167–2177. [[CrossRef](#)]
33. Blaacha, J.; Aboutni, R.; Aziz, A. A Comparative Study Between a Unipolar and a Bipolar PWM Used in Inverters for Photovoltaic Systems. In *International Conference on Electronic Engineering and Renewable Energy*; Springer: Berlin/Heidelberg, Germany, 2020, pp. 353–360.
34. Krishna, T.M.; Veni, K.; Babu, G.S.; Sushma, D.; Harish, C. Performance Evaluation of Induction Motor for Unipolar and Bipolar Pulse Width Modulation Techniques. *Int. J. Innov. Technol. Explor. Eng. (IJITEE)* **2019**, *8*, 3626–3629.
35. Behera, P.K.; Das, S.; Pattnaik, M. Performance Comparison Between Bipolar and Unipolar Switching Scheme for a Single-Phase Inverter Based Stand-alone Photovoltaic System. In Proceedings of the 2019 IEEE 16th India Council International Conference (INDICON), Rajkot, Gujarat, 13–15 December 2019; pp. 1–4.
36. Utkin, V.I.; Chang, H.C. Sliding mode control on electro-mechanical systems. *Math. Probl. Eng.* **2002**, *8*, 451–473. [[CrossRef](#)]
37. Utkin, V.; Guldner, J.; Shi, J. *Sliding Mode Control in Electro-Mechanical Systems*; CRC Press: Boca Raton, FL, USA, 2017.
38. Yasin, A.R.; Ashraf, M.; Bhatti, A.I. A novel filter extracted equivalent control based fixed frequency sliding mode approach for power electronic converters. *Energies* **2019**, *12*, 853. [[CrossRef](#)]